

Multidimensional Anodized Titanium Foam Photoelectrode for Efficient Utilization of Photons in Mesoscopic Solar Cells

Jin Soo Kang, Hyelim Choi, Jin Kim, Hyeji Park, Jae-Yup Kim, Jung-Woo Choi, Seung-Ho Yu, Kyung Jae Lee, Yun Sik Kang, Sun Ha Park, Yong-Hun Cho, Jun-Ho Yum, David C. Dunand, Heeman Choe, and Yung-Eun Sung**

Mesoscopic solar cells based on nanostructured oxide semiconductors are considered as a promising candidates to replace conventional photovoltaics employing costly materials. However, their overall performances are below the sufficient level required for practical usages. Herein, this study proposes an anodized Ti foam (ATF) with multidimensional and hierarchical architecture as a highly efficient photoelectrode for the generation of a large photocurrent. ATF photoelectrodes prepared by electrochemical anodization of freeze-cast Ti foams have three favorable characteristics: (i) large surface area for enhanced light harvesting, (ii) 1D semiconductor structure for facilitated charge collection, and (iii) 3D highly conductive metallic current collector that enables exclusion of transparent conducting oxide substrate. Based on these advantages, when ATF is utilized in dye-sensitized solar cells, short-circuit photocurrent density up to 22.0 mA cm^{-2} is achieved in the conventional N719 dye- I_3^-/I^- redox electrolyte system even with an intrinsically inferior quasi-solid electrolyte.

Dr. J. S. Kang, J. Kim, Dr. J.-W. Choi, Dr. S.-H. Yu, Dr. K. J. Lee,
Dr. Y. S. Kang, Dr. S. H. Park, Prof. Y.-E. Sung
Center for Nanoparticle Research
Institute for Basic Science (IBS)
Seoul 08826, Republic of Korea
E-mail: ysung@snu.ac.kr

Dr. J. S. Kang, J. Kim, Dr. J.-W. Choi, Dr. S.-H. Yu,
Dr. K. J. Lee, Dr. Y. S. Kang, Dr. S. H. Park, Prof. Y.-E. Sung
School of Chemical and Biological Engineering
Seoul National University
Seoul 08826, Republic of Korea

Dr. H. Choi, H. Park, Prof. H. Choe
School of Advanced Materials Engineering
Kookmin University
Seoul 02707, Republic of Korea
E-mail: heeman@kookmin.ac.kr

Prof. J.-Y. Kim
Department of Chemical Engineering
Hoseo University
Asan 31499, Republic of Korea

DOI: 10.1002/sml.201701458

Prof. Y.-H. Cho
Department of Chemical Engineering
Kangwon National University
Samcheok 25913, Republic of Korea
Dr. J.-H. Yum
Laboratory for Molecular Engineering of
Optoelectronic Nanomaterials
École Polytechnique Fédérale de Lausanne (EPFL)
Station 6, Lausanne 1015, Switzerland
Prof. D. C. Dunand
Department of Materials Science and Engineering
Northwestern University
Evanston, IL 60208, USA
Prof. H. Choe
Cellmotive Co. Ltd.
Kookmin University
Seoul 02707, Republic of Korea



 The ORCID identification number(s) for the author(s) of this article can be found under <https://doi.org/10.1002/sml.201701458>.

Dye-sensitized solar cells (DSCs) are highly efficient organic/inorganic hybrid photovoltaic systems with excellent reliability, and they are considered promising solar energy conversion devices due to their environmentally and economically favorable characteristics.^[1–4] Significant advances in electrolytes and light harvesters have been achieved in the last few years. For example, cobalt redox couples with compatible organic sensitizers have resulted in remarkable energy conversion efficiency with increased photovoltage,^[5–8] and perovskite materials have led to a new era of solid-state cells due to their outstanding light harvesting and charge transport properties.^[9–17] Various mesoscopic photoelectrodes with elaborate composition and structures have also been proposed;^[18–22] however, there have been no studies on the mesoscopic photoelectrode of an excitonic solar cell that surpasses the performance of TiO₂ nanoparticles (NPs), which thus far have been the best-performing photoelectrode since the inception of DSCs in 1991.^[1,8]

Though TiO₂ NPs have exceptional features, such as their large available surface area for high dye-loading for efficient light harvesting, they suffer from a significant degree of charge recombination, which leads to a considerable performance drop.^[4,23] To minimize recombination rates, 1D structures, such as nanotubes and nanowires, have been investigated in the search for a method to effectively confine

the pathways of conduction band electrons.^[24–33] Although these types of structural designs have reduced charge recombination rates to some extent, their overall cell performance was inferior to that of NP-based cells. The reason for this is mainly because these structures have a smaller surface area for light harvesting, leading to lower photocurrents compared with NPs.

Herein, we propose anodized Ti foam (ATF) as a new type of photoelectrode and investigate its application for DSCs. We first produced TiO₂ nanotube arrays (NTAs) on the surface of freeze-cast Ti foam via electrochemical anodization,^[34,35] which is a robust and simple process. After dye-sensitization, the resulting ATF was used directly as a transparent conducting oxide-free photoanode with ideal characteristics originating from its multidimensional architecture, such as a large surface area and low-dimensional semiconductor structure for enhanced light harvesting and charge transport, respectively. In addition, 3D metallic Ti beneath the TiO₂ NTAs served as an efficient current collector. As a result, the ATF in the DSCs generated a large photocurrent density of up to 22.0 mA cm⁻², verifying the general advantages of this design concept.

Figure 1a shows the schematic fabrication process of the ATF photoelectrode for DSCs. The Ti foam was prepared using the freeze-casting process,^[36] cut into slices, and

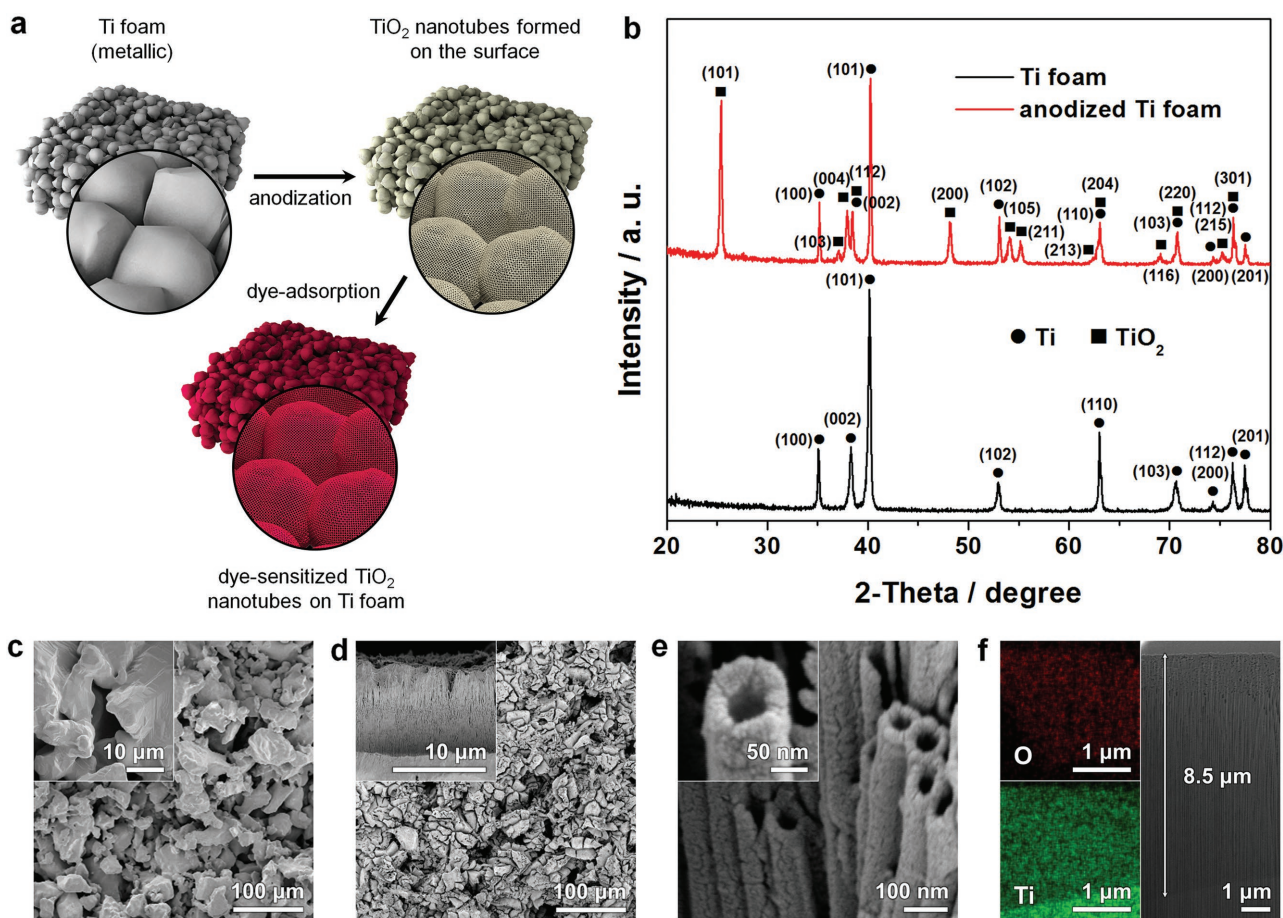


Figure 1. a) Schematic image displaying the fabrication of the ATF photoanode; b) XRD data of Ti foam before and after anodization followed by heat treatment at 450 °C for 4 h (the XRD peaks were assigned according to JCPDS 65–9622 (Ti) and 21–1272 (anatase TiO₂)); c) SEM images of Ti foam; and d–f) SEM images of the ATF.

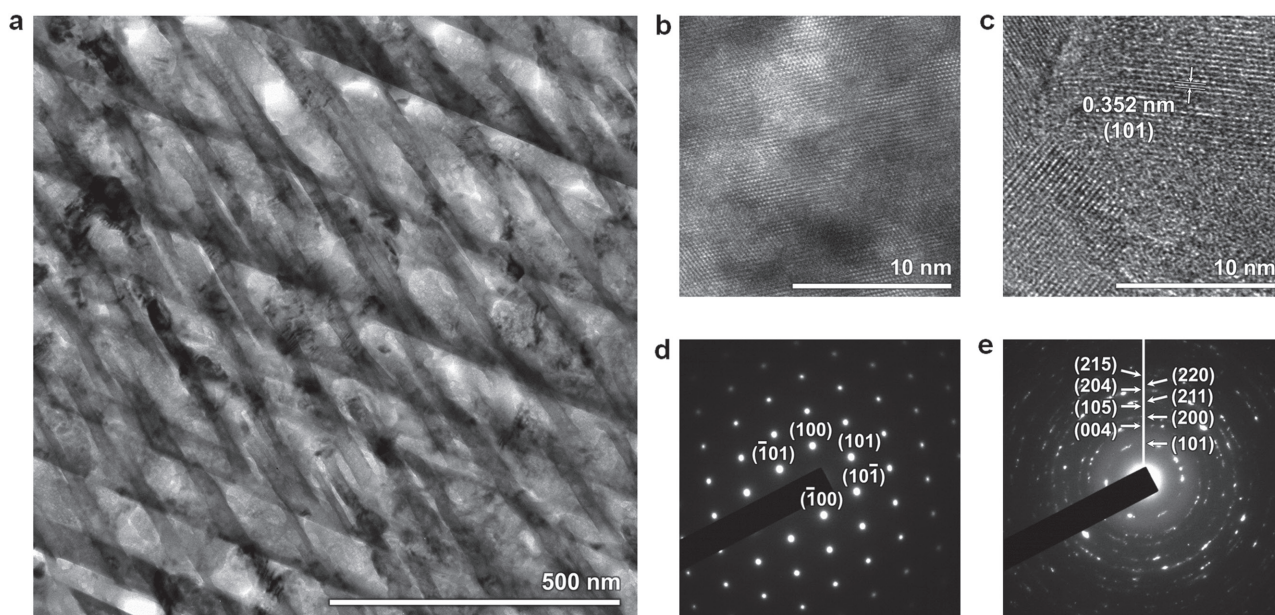


Figure 2. a) TEM image of ATF, and HR-TEM images of b) the Ti foam substrate and c) TiO₂ nanotubes and their corresponding SAED patterns d,e) on the surface of the ATF.

polished into thin foil with a uniform thickness of $\approx 500 \mu\text{m}$. Electrochemical anodization was carried out at 80 V for 30 min at 25 °C using ethylene glycol electrolyte containing 0.25 wt% NH₄F and 2 vol% H₂O. From the X-ray diffraction (XRD) patterns in Figure 1b, the formation of anatase TiO₂ is observable. Scanning electron microscope (SEM) images of Ti foam before (Figure 1c) and after anodization (Figure 1d–f) clearly show that NTAs are synthesized on the surface of the foam. In addition, a cross-sectional image of the Ti foam substrate beneath the TiO₂ NTAs was made after focused ion beam (FIB) milling (Figure 1f), and corresponding elemental energy dispersive spectroscopy maps (insets of Figure 1f) unveiled the existence of metallic Ti under the TiO₂ NTAs. Nanotubes had an outside diameter of $\approx 100 \text{ nm}$ and a wall thickness of 30 nm (Figure 1e), and their length at the ATF surface was $\approx 8.5 \mu\text{m}$ (Figure 1f). SEM examination on the fractured surface of the ATF confirmed that the TiO₂ NTAs were also formed on the inner surfaces (near the center) of the ATF (Figure S1, Supporting Information). Further characterization was carried out using transmission electron microscopy (TEM) on samples prepared using FIB milling (Figure 2a). High-resolution images and selected area electron diffraction (SAED) patterns of the internal metallic (Figure 2b,d) and external oxide parts (Figure 2c,e) indicate that monocrystalline (i.e., coarse-grained) Ti was located beneath the polycrystalline TiO₂. In addition, the lattice spacing in the oxide part was measured as 0.352 nm (Figure 2c), which matches the (101) plane of anatase TiO₂.

For the cell assembly, commercial quasi-solid electrolyte (EL-SGE, Dyesol) containing I₃⁻/I⁻ redox couples was used because we could not find a practical method to completely seal the lab-scale DSCs employing the ATF photoanode (ATF-DSCs). The schematic image and constitution of the ATF-DSCs are presented in Figure 3a and Figure S2 in the

Supporting Information, respectively. Conventional DSCs with TiO₂ NPs (NP-DSCs) were fabricated with an 8.5 μm thick TiO₂ NP film on fluorine-doped tin oxide (FTO) glass (Figure S3, Supporting Information). Pt-FTO was used as the counter electrodes, and N719 dyes were used as sensitizers for both types of DSCs. The photovoltaic performance of the DSCs was measured under standard AM 1.5G illumination. From the current density–voltage (J – V) characteristics (Figure 3b), significant differences in both short-circuit current density (J_{sc}) and open-circuit potential (V_{oc}) were observed. Replacing TiO₂ NPs with ATF decreased V_{oc} by 26.4% from 0.853 to 0.628 V but increased energy conversion efficiency by 12.5% (from 4.23% for the NP-DSCs to 4.76% for the ATF-DSCs). Most importantly, J_{sc} increased considerably from 7.4 to 22.0 mA cm^{-2} (details of photovoltaic performance are summarized in Table 1). This result is very promising given that the photocurrent and efficiency of quasi-solid DSCs are generally inferior to liquid-electrolyte DSCs, as clearly seen in Table S1 and Figure S4 in the Supporting Information.

There are a few noteworthy characteristics observed for the ATF-DSCs. First, the increase in photocurrent density was very substantial. A measured value of 22.0 mA cm^{-2} is one of the largest values of J_{sc} reported for DSCs with an N719 sensitizer.^[37] Moreover, according to the standard AM 1.5G solar spectrum, the maximum theoretical value of J_{sc} for the N719-sensitized solar cells is known as 25.3 mA cm^{-2} given that the onset wavelength of N719 dye is around 775 nm.^[38] Hence, a value of 22.0 mA cm^{-2} is more than 80% of the ideal value. Second, it is obvious that the V_{oc} and fill factor (FF) of the ATF-DSCs were low compared to the NP-DSCs, which is likely attributable to the small shunt resistance resulting from charge recombination.

The high photocurrent density of the ATF-DSCs is mainly attributable to enhanced light harvesting and current

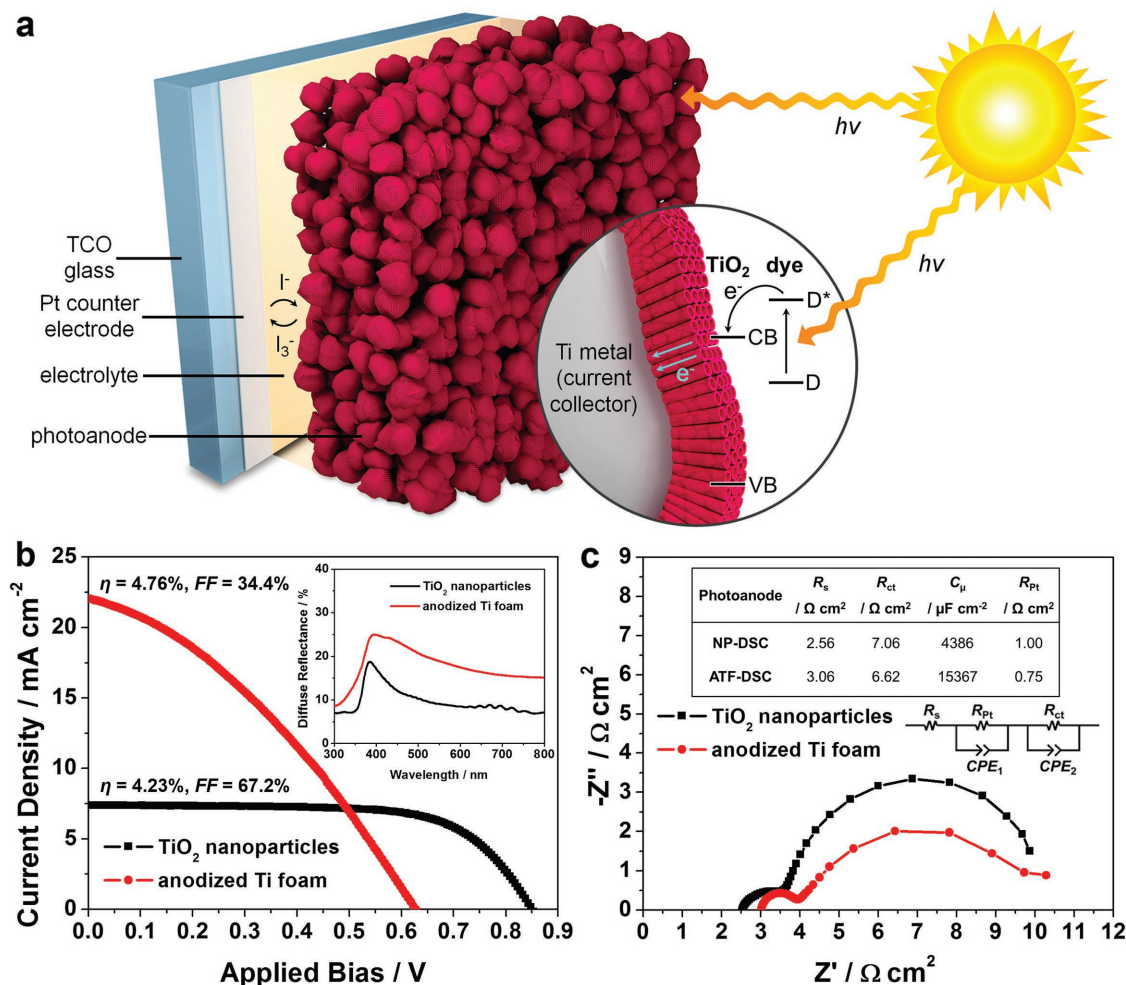


Figure 3. a) Schematic image of a DSC with ATF as the photoanode, b) J - V characteristics, and c) Nyquist plot for the best performing ATF-DSC and NP-DSC. The inset in Figure 2b shows the diffuse reflectance of NP-FTO and ATF, and the values in the inset table in Figure 2c are the fitted parameters from EIS measurements according to the presented equivalent circuit. The term “constant phase element” (CPE) generally represents the interfacial capacitance of a rough electrode surface.

collection. We compared the relative roughness factors of the ATF and the TiO₂ NP photoanode by measuring the comparative loading amount of dye. Remarkably, the amount of adsorbed dye molecules on the ATF was more than 25 times larger than that on the TiO₂ NPs (5.50×10^{-6} and 1.98×10^{-7} mol cm⁻² for the ATF and NPs, respectively). This indicates that there are more photoactive surfaces for light absorption and charge separation in the ATF than the TiO₂ NPs. According to previous reports, the average area occupied by a single N719 dye molecule is 1.6 nm² on the (101) surface plane of anatase TiO₂.^[39,40] By the calculations based on this value, we were able to obtain the roughness factors (i.e., total surface area per unit substrate area) of

the ATF and TiO₂ NPs as 52 994 and 1908, respectively. Considering that there are facets other than (101) exposed on the surface of the TiO₂ NPs and the ATF, the obtained values are approximations. However, roughness factors of $\approx 10 \mu\text{m}$ thick TiO₂ films composed of ≈ 20 nm sized NPs are known to be around 1500,^[41] and this indicates that the calculated roughness factors seem to be within a reasonable range.

As shown from the diffuse reflectance in the inset of Figure 3b, the ATF is superior to the NPs in terms of light scattering, which enables more efficient harvesting of photons. In addition, replacing the FTO glass with a glass slide at the front minimized light loss (Figure S5, Supporting Information) and resulted in the additional benefit of reducing the fabrication cost. Furthermore, in NP-DSCs, the FTO serves as a current collector with its sheet resistance being 7.9Ω square⁻¹, whereas in ATF-DSCs, the internal 3D Ti foam beneath the TiO₂ NTAs serves as a current collector with its sheet resistance being $12.4 \text{ m}\Omega$ square⁻¹. Moreover, a 1D TiO₂ structure has been experimentally proven to be superior in terms of charge transport to the mesoporous structure of TiO₂ NPs.^[26] As a consequence, current collection is much more effective in ATF-DSCs due to the

Table 1. J - V characteristics of the NP-DSCs and ATF-DSCs.

	V_{oc} [V]	J_{sc} [mA cm ⁻²]	FF [%]	η [%]
NP-DSC	0.853	7.4	67.2	4.23
ATF-DSC	0.628	22.0	34.4	4.76
(Average \pm S. D.)	(0.614 \pm 0.012)	(21.5 \pm 0.4)	(35.3 \pm 1.0)	(4.67 \pm 0.10)

unique structural characteristics and properties of the ATF photoanode design.

Meanwhile, the main reason for the low V_{oc} and FF appears to be the gaps present between the metallic Ti and the TiO_2 NTAs, which were observable in a number of edges of the ATF (see the SEM images displayed in Figure S6 in the Supporting Information). These interspaces may accelerate charge recombination because (i) the direct contact between the metallic Ti and the iodide redox electrolyte induces electron transfer (backward reaction) at the interface and (ii) the conduction band electrons in the TiO_2 do not reach the current collector within their lifetime. Additionally, we obtained the transmittance spectrum of the ATF (see Figure S7 in the Supporting Information) and discovered that ATF is completely opaque in the UV–vis wavelength region. This indicates that the photoactive oxides in the rear-most part of the ATF photoelectrodes were not able to participate in light harvesting, which means that the balance between the forward and backward reactions was probably tipped toward the latter in the rear part (the farthest region from the light source) of the ATF photoelectrodes, which appears to be another reason for the manifestation of low V_{oc} and FF. The presence of a passivation layer and reduction of the ATF's thickness are expected to suppress charge recombination,^[42] though they were not performed in the current study due to the limitations in uniform-shell formation and handling of the ATF photoelectrodes in lab-scale experiments.

Additional investigations on the interfacial charge transfer kinetics of the NP-DSCs and ATF-DSCs were carried out using electrochemical impedance spectroscopy (EIS). Figure 3c shows the Nyquist plot measured under AM 1.5G illumination and a forward bias of V_{oc} for each cell, showing high- and mid-frequency regions with the semicircles corresponding to the Pt-FTO/electrolyte and TiO_2 /electrolyte interfaces, respectively. The low-frequency range was not measured because of the significantly different mass transfer conditions (distances between the photoanode and counter electrode) for the two cells. However, the ATF-DSCs were expected to be superior in electrolyte diffusion owing to the hierarchical dual pore structure of the ATF with both micro- and nanoscale pores. The microscale pores (in the order of tens of micrometers) enabled redox couples to penetrate easily, whereas the NTAs (with a pore size in the order of tens of nanometers) provided better electrolyte mass transfer than the NPs.^[43]

In Figure 3c, the inset table shows the fitted values of the EIS data based on the inset equivalent circuit. The charge transfer resistance at the Pt-FTO/electrolyte interface (R_{Pt}) observed at the high frequency range was different by a factor of 1/4 between the NP-DSCs and ATF-DSCs because the evaluated parameters were affected by the applied bias potential. However, the difference in R_{Pt} values was considered insignificant because all counter electrodes were fabricated using exactly the same method. Series resistance (R_s) was larger in the ATF-DSCs than the NP-DSCs because of the longer distance between the photoanode and counter electrode, which resulted in a much larger ohmic resistance of the electrolyte in the ATF-DSCs (Figure S8, Supporting Information).

In the quasi-solid DSCs, a larger charge transfer resistance (R_{ct}) value generally indicates poorer interfacial contact between the photoelectrode and electrolyte.^[44] The similar R_{ct} values of the NP-DSCs and ATF-DSCs show that there was no significant difference in the contact. The largest difference was in the chemical capacitance (C_{μ}) at the TiO_2 /electrolyte interface (C_{μ} represents the degree of photo-injected electron accumulation in the TiO_2 conduction band). A threefold increase in C_{μ} for the ATF-DSCs suggests that a larger amount of excited electrons were produced in the ATF-DSCs as compared to the NP-DSCs. A large conduction band electron density contributes to a higher photocurrent generation, and the large increase showed a good match with the trend in the J_{sc} values. However, the charge recombination rate increased strongly with increasing electron density in the TiO_2 conduction band, resulting in a drop in V_{oc} because of the accelerated back reaction.^[45]

In summary, we designed ATF as a conceptually ideal photoelectrode for DSCs. The ATF in the DSCs resulted in a threefold improvement in photocurrent generation, and a photocurrent density as high as 22 mA cm^{-2} was observable under the standard AM 1.5G condition. Though the overall energy conversion efficiency was strongly affected by low FF, it is clear that there is room for further optimization in terms of surface modification and device architecture to minimize charge recombination. Owing to favorable characteristics such as a large surface area, 1D semiconductor nanostructure, and 3D metallic current collector, the advantages present in the ATF photoanodes are anticipated to bring advances to the current technology of mesoscopic solar cells.

Experimental Section

Preparation of Anodized Titanium Foam Photoelectrodes: Unalloyed Ti powder (Aremco) composed of particles of less than $45 \mu\text{m}$ in size was used. As had been reported elsewhere,^[36] a series of steps were carried out to prepare samples using the freeze-casting process. A dry mass of 4.9 g of Ti powder was added to 3.5 mL deionized, de-aired water contained within a cylindrical glass vessel of 13 mm inner diameter and 38 mm height, to which 0.2 wt% agar (as a binder) and 1 μL of neutral detergent (as a surfactant) were also added. After stirring the powder to form a slurry, the vessel was placed on a copper chiller block and kept at $-17 \text{ }^\circ\text{C}$ in a freezer. The side of the vessel was insulated with polystyrene foam to minimize radial heat loss. The frozen ice/Ti composite green body was lyophilized to remove the ice via sublimation using a freeze dryer at $-40 \text{ }^\circ\text{C}$ under a 7.5 Pa vacuum for around 24 h. The lyophilized green body was then sintered in a vacuum furnace through a two-step heat-treatment process: first at $300 \text{ }^\circ\text{C}$ for 3 h and subsequently at $877 \text{ }^\circ\text{C}$ for 5 h. More detail on the Experimental Section is available from a previous study.^[36] The specimens for anodization were obtained from the bottom region (near the chiller) of freeze-cast Ti foam with an equiaxed pore shape and $40 \pm 4\%$ porosity determined by image analysis on an SEM micrograph of a polished cross-section. A metallographic examination was carried out using both optical microscopy and SEM on ground and polished or fractured samples. After machining the fabricated foam to a uniform thickness of $500 \mu\text{m}$, it

was anodized at 80 V and 25 °C in ethylene glycol electrolyte containing 0.25 wt% NH₄F and 2 vol% H₂O for 30 min. The anodized foam was thermally annealed at 450 °C for 4 h for enhancement of crystallinity and was TiCl₄-treated to increase the roughness and injection efficiency.^[46,47] The ATF was subsequently immersed in an ethanol solution of 0.5 × 10⁻³ M *cis*-bis (isothiocyanato) bis (2,2'-bipyridyl-4,4-dicarboxylic acid) ruthenium (II) (N719 dye, highly purified, Ohyoung industry) for 48 h in order to place the sensitizers on the TiO₂ surface.

Fabrication of Dye-Sensitized Solar Cells: The platinum counter electrode was fabricated using a thermal decomposition method as previously reported elsewhere.^[48] Commercial gel-type electrolyte containing I₃⁻/I⁻ redox couples (EL-SGE, Dyesol) was pre-immersed into the DSCs prior to cell assembly by spring clamps. Fourteen layers of 50 μm thick thermoplastic gasket (Surlyn, Dupont) were used as a spacer without thermal annealing because of its chemical stability against the corrosive I₃⁻/I⁻ electrolyte. A transparent glass slide was placed on the outermost part of the photoanode to prevent leakage of electrolyte through the pores of the photoanode. The conventional mesoporous TiO₂ photoanode was prepared by application of commercial TiO₂ NP paste (DSL 18NR-T, Dyesol) onto FTO glass (TEC-8, Pilkington) using a doctor blade method followed by thermal sintering at 500 °C for 30 min, followed by TiCl₄ treatment and N719 sensitization. Loaded dye amounts on each type of electrode were measured from the absorbance peak at 535 nm measured after desorption of the dye in 1 M NaOH aqueous solution, and the number of dye molecules was calculated on the basis of an extinction coefficient of ε = 3748 cm⁻¹ M⁻¹ according to previous reports.^[49,50] Cell assembly was achieved with exactly the same method used for ATF-DSCs except for the thickness of the spacer, which was 50 μm for the NP-DSCs.

Characterization and Physical Measurements of the Materials: XRD data were measured using a Rigaku D-MAX2500-PC, and SEM images were taken with a Carl Zeiss SUPRA 55VP and a Carl Zeiss AURIGA. TEM analysis was carried out using JEOL JEM-2100F, and a specimen for cross-sectional observation was prepared using FIB milling (SMI3050SE, SII Nanotechnology). Absorbance, transmittance, and reflectance were measured using a UV-vis-NIR spectrophotometer (V-670, Jasco), and cell performance was characterized using a 500 W xenon isotope lamp (XIL; model 05A50KS source units) under the AM 1.5G condition (light intensity: 100 mW cm⁻²), which was adjusted by the Si reference cell certified by the National Institute of Advanced Industrial Science and Technology (AIST, Japan). A potentiostat (Solartron 1480 Multistat) was used for *J*-*V* measurements of the DSCs, and EIS analysis was carried out using a Zahner IM6 electrochemical workstation under AM 1.5G illumination with the forward bias of the open-circuit potential for each cell. Sheet resistance was measured using a four-point probe (CMT-SP 2000N, AIT).

Supporting Information

Supporting Information is available from the Wiley Online Library or from the author.

Acknowledgements

Y.-E.S. acknowledges financial support from the Institute for Basic Science (IBS) in Republic of Korea (Project Code: IBS-R006-G1 and IBS-R006-D1). H.C. acknowledges supports from the Basic Science Research Program (2014R1A2A1A11052513), and the Priority Research Centers Programs (2012-0006680) through the National Research Foundation (NRF) of Korea. The authors give thanks to Dr. Yasumasa Chino at Materials Research Institute for Sustainable Development, the National Institute of Advanced Industrial Science and Technology (AIST) in Japan for fabrication of the titanium foam during his stay in Northwestern University as a visiting scholar.

Conflict of Interest

The authors declare no conflict of interest.

- [1] B. O'Regan, M. Grätzel, *Nature* **1991**, 353, 737.
- [2] M. Grätzel, *Nature* **2001**, 414, 338.
- [3] M. Grätzel, *Acc. Chem. Res.* **2009**, 42, 1788.
- [4] A. Hagfeldt, G. Boschloo, L. Sun, L. Kloo, H. Pettersson, *Chem. Rev.* **2010**, 110, 6595.
- [5] S. M. Feldt, E. A. Gibson, E. Gabrielsson, L. Sun, G. Boschloo, A. Hagfeldt, *J. Am. Chem. Soc.* **2010**, 132, 16714.
- [6] A. Yella, H.-W. Lee, H. N. Tsao, C. Yi, A. K. Chandiran, M. K. Nazeeruddin, E. W.-G. Diao, C.-Y. Yeh, S. M. Zakeeruddin, M. Grätzel, *Science* **2011**, 334, 629.
- [7] S. Mathew, A. Yella, P. Gao, R. Humphry-Baker, B. F. E. Curchod, N. Ashari-Astani, I. Tavernelli, U. Rothlisberger, M. K. Nazeeruddin, M. Grätzel, *Nat. Chem.* **2014**, 6, 242.
- [8] K. Kakiage, Y. Aoyama, T. Yano, K. Oya, J.-i. Fujisawa, M. Hanaya, *Chem. Commun.* **2015**, 51, 15894.
- [9] H.-S. Kim, C.-R. Lee, J.-H. Im, K.-B. Lee, T. Moehl, A. Marchioro, S.-J. Moon, R. Humphry-Baker, J.-H. Yum, J. E. Moser, M. Grätzel, N.-G. Park, *Sci. Rep.* **2012**, 2, 591.
- [10] M. M. Lee, J. Teuscher, T. Miyasaka, T. N. Murakami, H. J. Snaith, *Science* **2012**, 338, 643.
- [11] J. Burschka, N. Pellet, S.-J. Moon, R. Humphry-Baker, P. Gao, M. K. Nazeeruddin, M. Grätzel, *Nature* **2013**, 499, 316.
- [12] P. Qin, S. Tanaka, S. Ito, N. Tetreault, K. Manabe, H. Nishino, M. K. Nazeeruddin, M. Grätzel, *Nat. Commun.* **2014**, 5, 3834.
- [13] W. S. Yang, J. H. Noh, N. J. Jeon, Y. C. Kim, S. Ryu, J. Seo, S. I. Seok, *Science* **2015**, 348, 1234.
- [14] P. Qin, M. Paulose, M. I. Dar, T. Moehl, N. Arora, P. Gao, O. K. Varghese, M. Grätzel, M. K. Nazeeruddin, *Small* **2015**, 11, 5533.
- [15] M. Park, H. J. Kim, I. Jeong, J. Lee, H. Lee, H. J. Son, D.-E. Kim, M. J. Ko, *Adv. Energy Mater.* **2015**, 5, 1501406.
- [16] S. S. Shin, E. J. Yeom, W. S. Yang, S. Hur, M. G. Kim, J. Im, J. Seo, J. H. Noh, S. I. Seok, *Science* **2017**, 356, 167.
- [17] Y. H. Park, I. Jeong, S. Bae, H. J. Son, P. Lee, J. Lee, C.-H. Lee, M. J. Ko, *Adv. Funct. Mater.* **2017**, 27, 1605988.
- [18] K. Park, Q. Zhang, B. B. Garcia, X. Zhou, Y.-H. Jeong, G. Cao, *Adv. Mater.* **2010**, 22, 2329.
- [19] J. Kim, J. K. Koh, B. Kim, J. H. Kim, E. Kim, *Angew. Chem. Int. Ed.* **2012**, 51, 6864.
- [20] S. H. Hwang, J. Yun, J. Jang, *Adv. Funct. Mater.* **2014**, 24, 7619.
- [21] J. Y. Lim, C. S. Lee, J. M. Lee, J. Ahn, H. H. Cho, J. H. Kim, *J. Power Sources* **2016**, 301, 18.

- [22] S. Jang, J. S. Kang, J.-K. Lee, S. M. Kim, Y. J. Son, A. Lim, H. Cho, J. Kim, J. Jeong, G. Lee, Y.-E. Sung, M. Choi, *Adv. Funct. Mater.* **2016**, *26*, 6584.
- [23] R. Jose, V. Thavasi, S. Ramakrishna, *J. Am. Ceram. Soc.* **2009**, *92*, 289.
- [24] J. M. Macák, H. Tsuchiya, A. Ghicov, P. Schmuki, *Electrochem. Commun.* **2005**, *7*, 1133.
- [25] G. K. Mor, K. Shankar, M. Paulose, O. K. Varghese, C. A. Grimes, *Nano Lett.* **2006**, *6*, 215.
- [26] K. Zhu, N. R. Neale, A. Miedaner, A. J. Frank, *Nano Lett.* **2007**, *7*, 69.
- [27] O. K. Varghese, M. Paulose, C. A. Grimes, *Nat. Nanotechnol.* **2009**, *4*, 592.
- [28] X. Feng, K. Shankar, O. K. Varghese, M. Paulose, T. J. Latempa, C. A. Grimes, *Nano Lett.* **2008**, *8*, 3781.
- [29] B. Liu, E. S. Aydil, *J. Am. Chem. Soc.* **2009**, *131*, 3985.
- [30] J.-K. Oh, J.-K. Lee, H.-S. Kim, S.-B. Han, K.-W. Park, *Chem. Mater.* **2010**, *22*, 1114.
- [31] J.-Y. Liao, B.-X. Lei, H.-Y. Chen, D.-B. Kuang, C.-Y. Su, *Energy Environ. Sci.* **2012**, *5*, 5750.
- [32] D. K. Roh, W. S. Chi, S. H. Ahn, H. Jeon, J. H. Kim, *ChemSusChem* **2013**, *6*, 1384.
- [33] S. So, I. Hwang, P. Schmuki, *Energy Environ. Sci.* **2015**, *8*, 849.
- [34] J. M. Macák, H. Tsuchiya, P. Schmuki, *Angew. Chem. Int. Ed.* **2005**, *44*, 2100.
- [35] H. E. Prakasam, K. Shankar, M. Paulose, O. K. Varghese, C. A. Grimes, *J. Phys. Chem. C* **2007**, *111*, 7235.
- [36] Y. Chino, D. C. Dunand, *Acta Mater.* **2008**, *56*, 105.
- [37] Y. Liu, R. Che, G. Chen, J. Fan, Z. Sun, Z. Wu, M. Wang, B. Li, J. Wei, Y. Wei, G. Wang, G. Guan, A. A. Elzatahry, A. A. Bagabas, A. M. Al-Enizi, Y. Deng, H. Peng, D. Zhao, *Sci. Adv.* **2015**, *1*, e1500166.
- [38] P. K. Nayak, J. Bisquert, D. Cahen, *Adv. Mater.* **2011**, *23*, 2870.
- [39] M. Grätzel, *Pure Appl. Chem.* **2001**, *73*, 459.
- [40] B. Tan, Y. Wu, *J. Phys. Chem. B* **2006**, *110*, 15932.
- [41] N. Alexaki, T. Stergiopoulos, A. G. Kontos, D. S. Tsoukleris, A. P. Katsoulidis, P. J. Pomonis, D. J. LeClere, P. Skeldon, G. E. Thompson, P. Falaras, *Micropor. Macropor. Mater.* **2009**, *124*, 52.
- [42] E. Palomares, J. N. Clofford, S. A. Haque, T. Lutz, J. R. Durrant, *J. Am. Chem. Soc.* **2003**, *125*, 475.
- [43] J.-Y. Kim, K. J. Lee, S. H. Kang, J. Shin, Y.-E. Sung, *J. Phys. Chem. C* **2011**, *115*, 19979.
- [44] Z. Chen, Y. Tang, H. Yang, Y. Xia, F. Li, T. Yi, C. Huang, *J. Power Sources* **2007**, *171*, 990.
- [45] S. E. Koops, B. C. O'Regan, P. R. F. Barnes, J. R. Durrant, *J. Am. Chem. Soc.* **2009**, *131*, 4808.
- [46] P. M. Sommeling, B. C. O'Regan, R. R. Haswell, H. J. P. Smit, N. J. Bakker, J. J. T. Smits, J. M. Kroon, J. A. M. van Roosmalen, *J. Phys. Chem. B* **2006**, *110*, 19191.
- [47] B. C. O'Regan, J. R. Durrant, P. M. Sommeling, N. J. Bakker, *J. Phys. Chem. C* **2007**, *111*, 14001.
- [48] N. Papageorgiou, W. F. Maier, M. Grätzel, *J. Electrochem. Soc.* **1997**, *144*, 876.
- [49] S. H. Kang, S.-H. Choi, M.-S. Kang, J.-Y. Kim, H.-S. Kim, T. Hyeon, Y.-E. Sung, *Adv. Mater.* **2008**, *20*, 54.
- [50] L. Cao, C. Wu, Q. Hu, T. Jin, B. Chi, J. Pu, L. Jian, *J. Am. Ceram. Soc.* **2013**, *96*, 549.

Received: May 6, 2017
Revised: June 13, 2017
Published online: